**Paper:**
Wang, M., Feng, Y. & Wang, C. (2017). Numerical investigation of initiation and propagation of hydraulic fracture using the coupled Bonded Particle–Lattice Boltzmann Method. *Computers & Structures, 181*, 32-40.
http://dx.doi.org/10.1016/j.compstruc.2016.02.014

# Numerical Investigation of Initiation and Propagation of Hydraulic Fracture Using the Coupled Bonded Particle-Lattice Boltzmann Method

*** Min Wang, Y. T. Feng and C. Y. Wang**

Zienkiewicz Centre for Computational Engineering, College of Engineering, Swansea University, Swansea, SA2 8PP

* sacewangmin@gmail.com

**Abstract**

This paper presents a coupled Bonded Particle and Lattice Boltzmann Method (BPLBM) for modelling fluid-solid interactions in engineering, e.g. geomechanics. In this novel technique, the Bonded Particle model is employed to describe the inter-particle interactions, and the bonds between contacted particles are assumed to be broken when the tensional force and/or tangential force reach a certain critical value; while the Lattice Boltzmann method is used to model the fluid phase, and the Immersed Moving Boundary (IMB) scheme is utilized to resolve the fluid-solid interactions. Based on this novel technique, the investigation of hydraulic fracturing is carried out. The onset and propagation of hydraulic fracture are successfully captured and reproduced. Numerical results show that the coupled BPLBM is promising and efficient in handling complicated fluid-solid interactions at the grain level in hydraulic fracturing.

**Keywords**

Hydraulic fracturing; Discrete Element Method; Bonded Particle Method; Lattice Boltzmann Method; Fluid-solid interaction

## 1 Introduction

Hydraulic fracturing is nowadays widely used to represent a process by which a fracture initiates and propagates due to hydraulic loading applied by a fluid inside the fracture. The application of hydraulic fracturing is abundant in geomechanics. Hydraulic fracturing began as a reservoir stimulation technique for oil exploitation in petroleum engineering. It was then used for hydrocarbon reservoir, shale oil production and geothermal energy extraction. The success of fracture stimulation is largely dependent on the size, shape and propagation behaviour of the created hydraulic fracture. Due to its complexity, the simulation of hydraulic fracturing has been a challenging research topic.

A good hydraulic fracturing model should include the mechanical deformation and fracturing propagation of the solid, the flow of the fluid within the fracture and the fluid pressure applied to the solid. Over the last decade, effort has been made and a number of numerical models have been proposed for the study of hydraulic fracturing. The computational fluid dynamics is the commonly used fluid solver. From the solid point of view, the Boundary Element Method (Luchi and Rizzuti, 1987), based on a weakly-singular, weak-form traction boundary integral equation, is the most popular approach (Carter et al., 2000, Hossain and Rahman, 2008). An alternative is the combined Finite-Discrete Element Method (Munjiza et al., 1995, Owen and Feng, 2001). This method treats the solid domain of interest as continuum at the beginning. When the simulation progresses, typically through explicit integration of the equations of motion, new discontinuities are allowed to form upon satisfying some fracture criterion, thus leading to the formation of new discrete bodies (Fu et al., 2013). The Extended Finite Element Method (XFEM) (Moës et al., 1999), based on the generalized finite element method (GFEM) and the partition of unity method (PUM), is another approach. It extends the classical finite element method (FEM) approach by enriching the solution space for solutions to differential equations with discontinuous functions (Mohammadnejad and Khoei, 2013, Chen, 2013). The latest technique for hydraulic fracturing is based on the numerical manifold method (Ma et al., 2009); there are two kinds of covers, namely mathematical cover and physical cover. With these two kinds of cover, the method is quite suitable for modelling discontinuous problems (Zhang et al., 2015).

In this work, a coupled Bonded Particle and Lattice Boltzmann Method (BPLBM) is proposed for the investigation of hydraulic fracturing. This novel technique, combining the Bonded Particle Method and the Lattice Boltzmann Method, is an extension of the Discrete Element – Lattice Boltzmann Method (DEM-LBM) (Feng et al., 2007, Han et al., 2007, Strack and Cook, 2007). Not only can it better simulate the mechanical response of geomaterials where cohesion forces exist between the bonded particles, but also tackle interactions between the granular particles and the fluid with high accuracy. It addresses fluid-particle issues at the grain-level commonly ranging from hundreds of microns to several centimetres.

The paper is organised as follows. In the next section a brief introduction of the Bonded Particle Method (BPM) is given, followed by the elaboration of the Lattice Boltzmann Method and the coupling of BPM and LBM. Then, validation of this coupling technique is performed and a hydraulic fracturing case in underground excavation is simulated using this coupled method and the initiation and propagation of fracture are captured at the microscale. Finally, it ends with conclusions and future work on how to improve this coupling method.

## 2 Computational Methodology

In this section, we shall introduce the framework of the coupled BPLBM. In this method, the solid comprising bonded particles or granular particles is modelled by BPM in which the cohesion forces between bonded particles are considered by the contact bond model (Potyondy and Cundall, 2004) and the fluid flow is solved using LBM with incorporation of the turbulence model (Feng et al., 2007).

In addition, the fluid-solid interactions are achieved through the immersed moving boundary (IMB) scheme (Noble and Torczynski, 1998) which is commonly used in DEM-LBM.

**2.1 Bonded Particle Method**

It has been noted that the bonds existing between adjacent particles can resist both traction and shear forces and will break due to excessive traction and/or shear forces (Delenne et al., 2004, Jiang et al., 2012). Therefore, the bonds play a vital role in determining the critical strength and force-displacement behaviour of geomaterials. Nowadays BPM is being extensively used for simulating brittle materials i.e. soil, rock and concrete. The concept of BPM is firstly proposed for rock by Potyondy and Cundall (2004). It originates from the Discrete Element Method (DEM) which has been proved to be an effective numerical tool for modelling problems consisting of granular particles. In BPM, the bond model mimicking cementation can be implemented between the particles in contact, and the bonds are able to carry normal forces, tangential forces and moment. When the bond force exceeds a critical value, the contact bond will break. In this case, only the particle-particle contact forces (independent of the bond) need to be considered.

The treatment of interactions between particles in this method is similar to that in the Discrete Element Method (Cundall and Strack, 1978, Cundall and Strack, 1979) in which particle-particle interactions are treated as a transient problem where an equilibrium state is reached when the internal forces are balanced. Newton's second law is utilised to determine the translation and rotation of each particle arising from the contact forces, e.g., externally applied forces and body forces as well as cohesive forces, while the force-displacement law is used to update the contact forces that keep changing due to the relative motion of particles at each contact. The dynamic behaviour is represented numerically by a time-stepping algorithm in which the velocities and accelerations are assumed to be constant within each time step. Because the propagation speed of disturbances is a function of the physical properties of the discrete medium, a sufficiently small time step should be chosen so that, in one time step, disturbances cannot propagate from a particle farther than its neighbouring particles. Therefore, at all times the resultant forces on any particle are determined exclusively by the neighbouring particles in contact.

Newton's second law governing the motion of a particle is given by

$$ma + cv = F_c + F_f + mg \tag{1}$$

$$I\ddot{\theta} = T_c + T_f \tag{2}$$

where $m$ and $I$ are respectively the mass and the moment of inertia of the particle; $c$ is a damping coefficient; $a$ and $\ddot{\theta}$ are respectively the acceleration and angular acceleration; $F_c$ and $T_c$ are respectively the contact forces and corresponding torques; $F_f$ and $T_f$ are the hydrodynamic force and torques. It should be emphasized that $F_c$ can be either particle-particle contact forces for granular particles or cohesion forces $F_b$ existing between bonded particles.

### 2.1.1 The particle-particle contact model

The particle-particle contact force $F_c$ has two components, the normal contact force and tangential contact force, which are, respectively, given by

Normal interaction laws: $F_n = K_n \delta^m$ (3)

Coulomb friction model:

$$F_t = -\frac{\dot{\delta}_t}{\left|\dot{\delta}_t\right|} \begin{cases} K_t\left|\delta_t\right|; & \left|K_t \delta_t\right| \leq \mu F_n \\ \mu F_n; & \left|K_t \delta_t\right| > \mu F_n \end{cases} \quad (4)$$

where $K_n$ and $K_t$ are respectively the normal stiffness and tangential stiffness; $\delta_t$ and $\dot{\delta}_t$ correspond to accumulated tangential sliding and sliding velocity; $\delta$ is the overlap of two particles. The coefficient $m$ can be 1 or 3/2; the former is for the linear contact and the latter is for the Hertz contact model.

### 2.1.2 The contact bond model

The bond model used in this work is referred to as the contact bond model (Itasca Consulting Group Inc, 2002, Potyondy and Cundall, 2004). It approximates the physical behaviour of a vanishingly small cemented-like substance joining the two bonded particles. It can be envisioned as a pair of elastic springs (or a point of glue) with constant normal and shear stiffness acting at the contact point. These two springs have specified shear and tensile strength. The existence of a contact bond precludes the possibility of slip. This widely accepted bond model accounts for forces acting at the contact point, but it is unable to undertake moment. Thus more advanced bond models are required to simulate more complicated mechanical behaviours (Potyondy and Cundall, 2004, Potyondy, 2007, Jiang et al., 2012, Jiang et al., 2014).

The contact bond is characterized by two parameters: normal bond strength ($F_{bn}$) and shear bond strength ($F_{bs}$). If the tensile contact force equals or exceeds the normal contact bond strength, the bond breaks, and both the normal and shear contact forces are set to be zero. However, when the shear contact force is equal or greater than the shear contact bond strength, the bond breaks, but the contact forces do not change. The contact bond model can be described by

Normal component:

$$F_n^b = \begin{cases} K_n^b \delta; & F_n^b \leq F_{\max} \\ 0; & F_n^b > F_{\max} \end{cases} \quad (5)$$

Tangential component: $$F_t^b = -\frac{\dot{\delta}_t}{\left|\dot{\delta}_t\right|}\begin{cases} K_t^b\left|\delta_t\right|; & \left|K_t^b\delta_t\right| \le \mu F_n^b \\ \mu F_n^b; & \left|K_t^b\delta_t\right| > \mu F_n^b \end{cases} \quad (6)$$

where $K_n^b$ and $K_t^b$ are respectively the normal stiffness and tangential stiffness for the cement; and $F_{\max}$ is the critical tensile force.

### 2.1.4 The general algorithm of BPM

The computational procedure of the Bonded Particle Method is briefly summarised as follows:

1). A particle packing with a specified size distribution will be generated first. Then, the first contact detection will be performed to build up a contact list for particles in contact. At the meantime, the overlaps between these contacting particle pairs are recorded. Then, bond models will be introduced to the particles according to the first contact detection;

2). When bond models are introduced, relaxation of the particle sample to a balanced state is required. Here a reduced-overlap method is proposed to secure a fast relaxation of a sample. At each time step, the deformation of the bond will be subtracted by the initial overlap record in the first step;

3). Next, the boundary conditions will be applied for the first time-step calculation and carry out the global contact detection and work out the overlap between contact particles for the subsequent contact force calculation;

4). Then check whether these contact pairs are on the bond contact list; if yes, use the contact bond model to calculate the cohesion forces between the bonded particles; otherwise calculate contact forces between no bonded pairs using the particle-particle contact models;

5). Check the calculated bond forces, if the tensile force or shear force exceeds its critical value, remove these contact pairs from the bond contact list;

6). Use the central difference time stepping scheme to update the position and velocity of each particle;

7). Repeat Steps 3-6 till the specific time interval is exceeded and output the useful data for postprocess.

The principal issues in BPM are the calculation of contact forces and the contact detection. The processing of contact forces has been introduced in this paper. Detailed discussion of contact detection algorithms can be found in the literatures (Feng and Owen, 2002, Munjiza, 2004). Considering the efficiency in terms of CPU and memory, we used the No Binary Search (NBS) (Munjiza and Andrews, 1998, Munjiza, 2004) contact detection algorithm in this work.

### 2.2 Lattice Boltzmann Method

The Lattice Boltzmann method is a modern approach in Computational Fluid Dynamics (CFD). In the conventional CFD, the fluid phase is treated as continuum. The primary variables are pressure, velocity and density. Its governing equations are the well-known Navier-Stokes (N-S) equations. In LBM the fluid domain is divided into regular lattices. The fluid phase is treated as a group of (imaginary) particle packages that residence at the lattice nodes. Each particle package includes several particles, such as 9 particles in the commonly used D2Q9 model. The flow of fluid can be achieved through resolving the particle collision and streaming. The Lattice Boltzmann Equation (LBE) is used to solve the streaming and collision process of fluid particles. The variable of LBM is the fluid density distribution function instead of pressure, density and velocity in the conventional CFD. Both mass and momentum of fluid particles are characterised by fluid density distributions. In particular, the N-S equation can be recovered from the LB equation under the condition of low Mach number (Chen et al., 1992).

The LBM is originated from Lattice Gas Automata (LGA) developed to eliminate the statistical noise. The first Lattice Boltzmann model is called the MZ model (McNamara and Zanetti, 1988), where the density distribution functions instead of Boolean variables were employed for particle treatment. It was then simplified to the HJ model by Higuera and Jiménez (1989) through linearizing the collision operator. The technique, however, suffers from poor numerical stability. To solve the problem, the HSB model was proposed (Higuera et al., 1989). Since the collision operator in the HSB model is out of the collision rule in LGA, the technique is deemed as a great progress in the model development. Two years later, the BGK model was proposed to simplify the collision operator in the HSB model, and it is a single relaxation model as only one relaxation parameter is introduced in the collision process (Chen et al., 1991, Chen et al., 1992). Subsequently, the MRT model was developed where multiple relaxation parameters are introduced (d'Humieres et al., 2002). The MRT model is better than BGK model in terms of accuracy and stability but its computational cost is higher.

#### 2.2.1 Bhatnagar-Gross-Krook (BGK) model

Given the computational efficiency and ease in programming, the BGK model is adopted in this work. It can be characterised by the following Lattice Boltzmann Equation:

$$f_i(\boldsymbol{x} + \boldsymbol{e}_i \Delta t, t + \Delta t) - f_i(\boldsymbol{x}, t) = \Omega \tag{7}$$

where $f_i$ is the primary variables in the LB formulation (so-called fluid density distribution functions), and $\Omega$ is the collision operator. In the BGK Model, $\Omega$ is characterised by a relaxation time $\tau$ and the equilibrium distribution function $f_i^{eq}(x, t)$

$$\Omega = -\frac{\Delta t}{\tau}\left[f_i(\boldsymbol{x},t) - f_i^{eq}(\boldsymbol{x},t)\right] \tag{8}$$

To make further explanation about LBM, we will take the widely used 2-D LB discretization scheme, the so-called D2Q9 model, as an example.

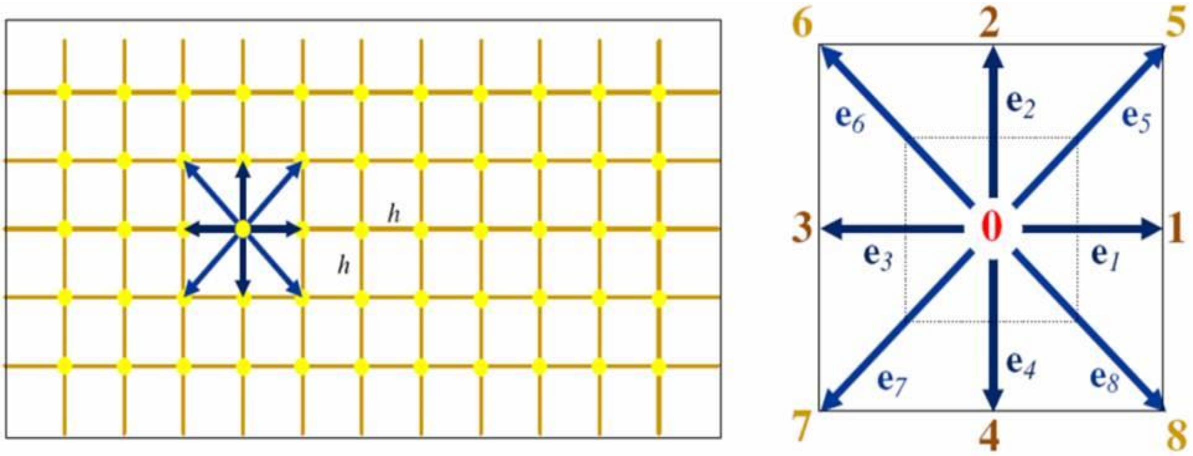


Fig. 1 LB discretization of a rectangular domain (left) and D2Q9 model (right)

The fluid domain is discretized into square lattices with side *h*. Particles at each node are allowed to move to its eight immediate neighbours with different velocities $e_i$ (i = 1,2,..,8). A proportion of the particles can rest at the node with a zero velocity $e_0$. As shown in Fig. 1, the nine discrete velocity vectors in total are defined as

$$e_0 = (0,0)$$

$$e_i = C(\cos\frac{\pi(i-1)}{2}, \sin\frac{\pi(i-1)}{2}) \qquad (i = 1,\ldots,4) \tag{9}$$

$$e_i = C(\cos\frac{\pi(2i-9)}{4}, \sin\frac{\pi(2i-9)}{4}) \qquad (i = 5,\ldots,8)$$

in which C is the lattice speed and is related to the lattice spacing, h, and the time step, $\Delta t$

$$C = h / \Delta t$$

The central issue to LBM is to control the movement of fluid particles via the density distribution functions. The evolution of the density distribution functions at each time step is governed by Equation 13. The equilibrium distribution function can be defined as

$$f_i^{eq} = \omega_i \rho(1 + \frac{3}{C^2} e_i \cdot v + \frac{9}{2C^4}(e_i \cdot v)^2 - \frac{3}{2C^2} v \cdot v) \qquad (i = 0,\ldots,8) \tag{10}$$

where $\rho$ and $v$ are the macroscopic fluid density and velocity, respectively and $\omega_i$ are the weighting factors:

$$\omega_0 = \frac{4}{9}, \quad \omega_{1,2,3,4} = \frac{1}{9}, \quad \omega_{5,6,7,8} = \frac{1}{36} \tag{11}$$

The macroscopic fluid density $\rho$ and velocity $v$ can be calculated from the distribution functions

$$\rho = \sum_{i=0}^{8} f_i, \quad \rho \boldsymbol{v} = \sum_{i=1}^{8} f_i \boldsymbol{e}_i \tag{12}$$

The fluid pressure is given by

$$P = C_S^2 \rho \tag{13}$$

where $C_S$ is termed the fluid speed of sound and is related to the lattice speed C

$$C_S = C / \sqrt{3} \tag{14}$$

The kinematic viscosity, $\upsilon$, of the fluid is implicitly determined by

$$\upsilon = \frac{1}{3}(\tau - \frac{1}{2})\frac{h^2}{\Delta t} = \frac{1}{3}(\tau - \frac{1}{2})Ch \tag{15}$$

### 2.2.2 Turbulence modelling

Although LBM has been proved to be efficient for a variety of fluid flow with low Reynolds number, not much work has been done on the modelling of turbulent flow using LBM except a previous study (Huidan et al., 2005). However, the turbulent flow is common in hydraulic fracture (Tsai and Rice, 2010, Tsai and Rice, 2012, Ames and Bunger, 2015). The fracturing fluid pumped during the process is generally in turbulent flow. Besides, turbulent flow has been observed in experiments of fracture flow (Qian et al., 2007).

Large Eddy Simulation (LES) is a well-known turbulence modelling approach in the engineering field, which enables one to directly solve large spatial-scale turbulent eddies that carry the majority of the energy. The smaller-scale eddies are described by using a subgrid model. The separation of these scales is achieved through filtering the Navier–Stokes equations, from which solutions to the resolved scales are obtained. In this study, the one-parameter Smagorinsky subgrid model (Smagorinsky, 1963) is adopted, where the Reynolds stress tensor is assumed to be dependent only on the local strain rate.

A simple route to incorporate turbulence model is to directly apply the concept of LES to the LB formulation (Huidan et al., 2005). Following this approach, the filtered form of the LB equation is expressed as

$$\tilde{f}_i(\boldsymbol{x} + \boldsymbol{e}_i \Delta t, t + \Delta t) - \tilde{f}_i(\boldsymbol{x}, t) = -\frac{1}{\tau_*}\left[\tilde{f}_i(\boldsymbol{x}, t) - \tilde{f}_i^{eq}(\boldsymbol{x}, t)\right] \tag{16}$$

where $\tilde{f}_i$ and $\tilde{f}_i^{eq}$ represent the distribution function and the equilibrium distribution function of the resolved scales, respectively. The effect of the unresolved scale motion is modelled through an effective collision relaxation time scale $\tau_t$. Thus the total relaxation time $\tau_*$ is described by

$$\tau_* = \tau + \tau_t \tag{17}$$

where $\tau$ and $\tau_t$ are the relaxation times corresponding to the fluid viscosity $\upsilon$ and the turbulence viscosity $\upsilon_t$, respectively. Accordingly, $\upsilon_*$ is given by

$$\upsilon_* = \upsilon + \upsilon_t = \frac{1}{3}(\tau_* - \frac{1}{2})\frac{h^2}{\Delta t} = \frac{1}{3}(\tau + \tau_t - \frac{1}{2})C^2 \Delta t \tag{18}$$

$$\upsilon_t = \frac{1}{3}\tau_t C^2 \Delta t \tag{19}$$

where the turbulence viscosity $\upsilon_t$ is calculated in terms of the filtered strain rate tensor $\tilde{S}_{ij}$ and a filter length scale *h*

$$\upsilon_t = (S_c h)^2 \hat{S} \tag{20}$$

$$\hat{S} = \frac{\hat{Q}}{2\rho C_S^2 \tau_*} \tag{21}$$

in which $S_c$ is the Smagorinsky constant; $\hat{S}$ is the characteristic value of the filtered strain rate tensor $\tilde{S}_{ij}$, and $\hat{Q}$ is the filtered mean momentum flux can be computed from second-order moments $\tilde{Q}_{ij}$, with

$$\hat{S} = \sqrt{\sum_{i,j} \tilde{S}_{ij}\tilde{S}_{ij}}\ ; \quad \hat{Q} = \sqrt{2\sum_{i,j} \tilde{Q}_{ij}\tilde{Q}_{ij}}$$

Consequently, the turbulence relaxation time $\tau_t$ is obtained as

$$\tau_t = \frac{1}{2}(\sqrt{\tau^2 + 18(S_C h)^2(\rho C^4 \Delta t)^{-1}\hat{Q}} - \tau) \tag{22}$$

This extended LBM including turbulent flows is simple to implement and has been proved promising for turbulence simulations (Huidan et al., 2005) and was first introduced into the DEM-LBM in (Feng et al., 2007).

### 2.3 The Fluid-Solid Interactions

The fluid-solid interaction is a primary issue in the fluid-particle systems especially when a large number of particles are involved. In order to correctly model the fluid-solid interaction, the no-slip condition must be satisfied, in which the fluid and solid should have the same velocity at the fluid-solid interface. For a stationary particle, this no-slip condition can be easily imposed by the well-known bounce-back rule. Later a modified bounce-back rule was proposed for moving particle-fluid interaction (Ladd, 1994, Ladd and Verberg, 2001).

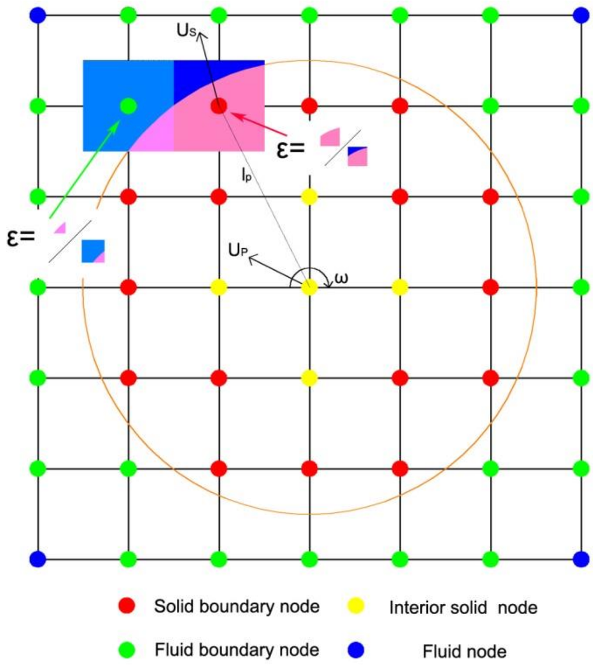


Fig. 2 IMB scheme and definition of local solid ratio ε

In order to resolve the problems in the Modified Bounce-back Rule for moving particles, Noble and Torczynski (1998) proposed a new boundary scheme, in which the particle is represented by solid nodes, the solid boundary nodes and interior solid nodes. The fluid nodes near the solid boundary nodes are defined as fluid boundary nodes. A diagram of IMB is plotted in Fig. 2 as an illustration. Four sorts of nodes, solid boundary nodes, interior solid nodes, fluid boundary nodes and normal fluid nodes, are, respectively, marked in red, yellow, green and blue. The fluid-solid coupling is achieved by dealing with the interactions between the fluid boundary nodes and the solid boundary nodes. In order to retain the advantages of LBM, namely the locality of the collision operator and the simple linear streaming operator, an additional collision term, $\Omega_i^s$, for nodes covered partially or fully by the solid is introduced to the standard collision operator of LBM. The modified collision operator for resolving the fluid-solid interaction is given by

$$\Omega = -\frac{\Delta t}{\tau}(1 - B)\left[f_i(\boldsymbol{x}, t) - f_i^{eq}(\boldsymbol{x}, t)\right] + (1 - B)\Delta t F_i + B\Omega_i^S \tag{23}$$

where B is a weighting function that depends on the local solid ratio $\varepsilon$, defined as the fraction of the solid node area to a cell area (see Fig. 2):

$$B = \frac{\varepsilon(\tau - 0.5)}{(1 - \varepsilon) + (\tau - 0.5)} \tag{24}$$

When $\varepsilon = 0$, B=0; and $\varepsilon = 1$, B=1.

The additional collision term is based on the bounce-rule for the non-equilibrium part and is given by

$$\Omega_i^S = f_{-i}(\boldsymbol{x}, t) - f_i(\boldsymbol{x}, t) + f_i^{eq}(\rho, \boldsymbol{U}_S) - f_{-i}^{eq}(\rho, \boldsymbol{u}) \tag{25}$$

where $U_S$ is the velocity of the solid node at time step $t + \Delta t$

$$\boldsymbol{U}_S = \boldsymbol{U}_p + \omega \times \boldsymbol{l}_C \qquad \left(l_C = \sqrt{(\boldsymbol{x} - \boldsymbol{x}_C)^2 + (\boldsymbol{y} - \boldsymbol{y}_C)^2}\right) \tag{26}$$

The resultant hydrodynamic force and torque exerted on the solid can be calculated by

$$\boldsymbol{F}_f = Ch\left[\sum_n (B_n \sum_i \Omega_i^s \boldsymbol{e}_i)\right] \tag{27}$$

$$\boldsymbol{T}_f = Ch\left\{\sum_n \left[(\boldsymbol{x} - \boldsymbol{x}_C) \times (B_n \sum_i \Omega_i^s \boldsymbol{e}_i)\right]\right\} \tag{28}$$

Later this method was modified by Holdych (2003). The modified version is as follows

$$\Omega_i^S = f_{-i}(\boldsymbol{x}, t) - f_i(\boldsymbol{x}, t) + f_i^{eq}(\rho, \boldsymbol{U}_S) - f_{-i}^{eq}(\rho, \boldsymbol{U}_S) \tag{29}$$

The only difference from the original version is that the solid velocity is used to calculate the equilibrium distribution for the last term. The modified IMB was validated and proved to be better in calculating the hydrodynamic forces for stationary particles (Strack and Cook, 2007, Jones, 2013). In addition, this scheme can recover the classic Bounce-Back rule for stationary particles; while at B=0 it reduces to the standard LB equation. However, it is found that there is a non-convergence problem with the modified IMB scheme for the fluid-moving particle interaction. Therefore, the original IMB scheme is adopted in the following simulation.

## 3 Model Validation

To demonstrate the accuracy and efficiency of the proposed fluid-particle coupling scheme, the extensively investigated benchmark (single particle sedimentation in viscous fluid) is carried out.

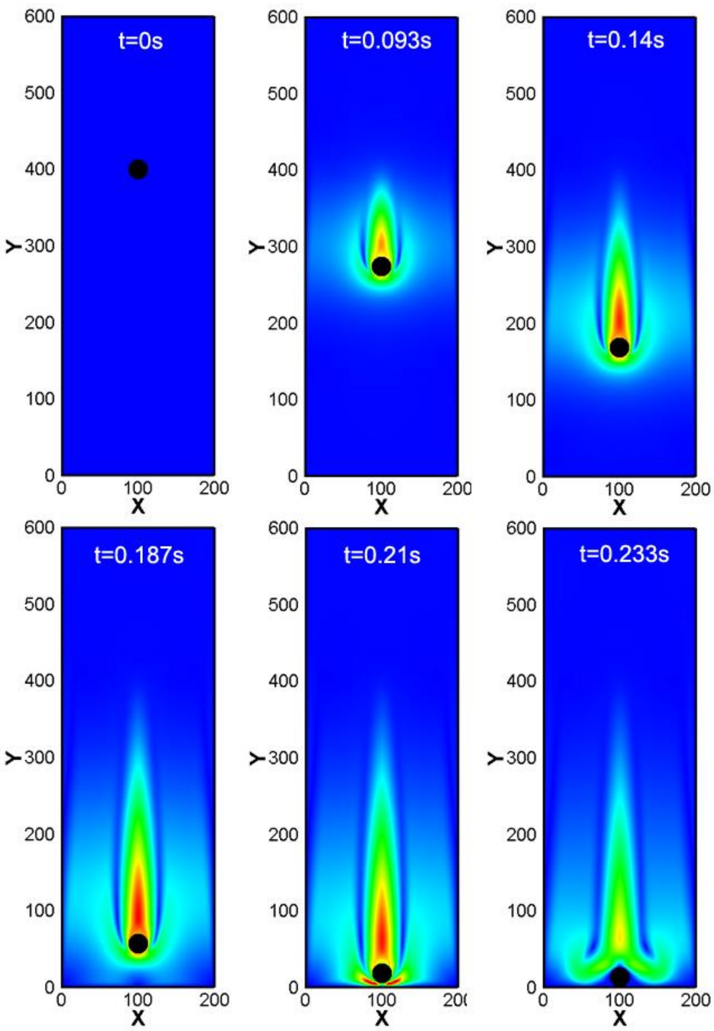


Fig. 3 Total velocity contour at different stages

In our simulation, a water-filled tube in 2 cm diameter (X-direction) and 6 cm height (Y-direction) is used. The fluid domain is divided into 200×600 square lattices with spacing h=0.1 mm. The kinematic viscosity and density of fluid are $1.0\times10^{-6}$ $m^2/s$ and 1000 $kg/m^3$, respectively. The density of the solid particle is 3000 $kg/m^3$, and its radius is 0.125 cm. Four boundaries of this simulation are stationary walls and thus the no-slip boundary condition is imposed. Initially, the particle is positioned at (1cm, 4cm) with the static state. Due to gravity force, the particle will go down. The Immersed Moving Boundary scheme is employed to resolving the particle-fluid interaction. The sedimentation process and fluid velocity contours of fluid at different time stages, 0.093s, 0.14s, 0.187s, 0.21s, 0.233s, are given in Fig. 3. To demonstrate the accuracy of IMB, the same simulation using the implicit velocity correction based IB-LBM (Dash et al., 2014) instead of IMB scheme is carried out. The evolution of particle movement in vertical direction and hydrodynamic forces applied to the particle with respect to time are compared in Figs. 4 and 5.

From Figs. 4 and 5, we can find that the motions of the particle simulated by the IMB and IBM schemes match very well. At the beginning, the particle falls down as an accelerated motion due to gravity force. After a distance it will sink with a constant speed as the gravity force, hydrodynamic force and buoyancy reach an equilibrium state. It is noticed that the hydrodynamic force calculated by IMB evolves smoothly except one point where the particle collides the bottom boundary. While, the drag forces obtained from IB scheme fluctuate around those calculated by IMB with the development of time. Sometimes, there are some fluctuations of hydrodynamic forces in the IB-LBM proposed by (Dash et al., 2014).

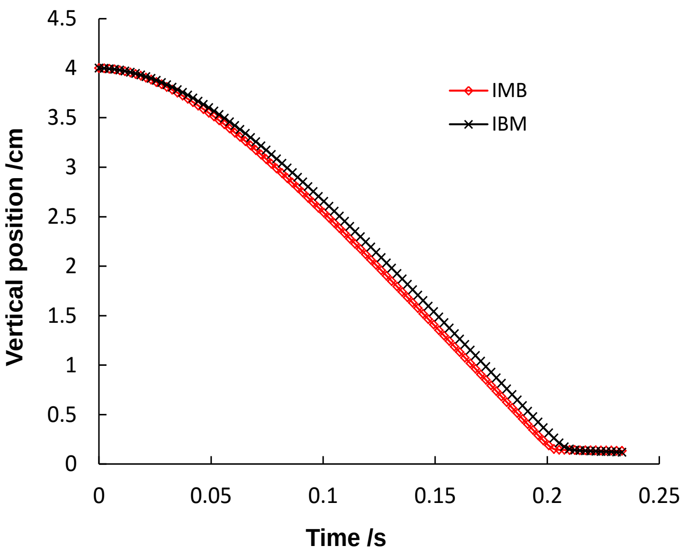


Fig. 4 Comparison of particle movement in Y direction

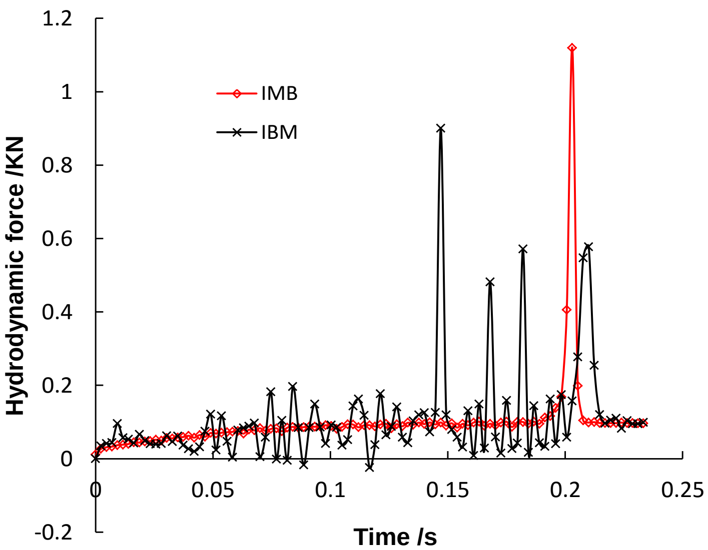


Fig. 5 Comparison of drag forces applied to particle

## 4 Numerical Tests

A hydraulic fracture process triggered by the horizontal directional drilling in an underground construction is investigated. The model with dimensions $1\,m \times 1\,m$ is shown in Fig. 6 (t=0s) and it is comprised of 3828 bonded particles of 4 different radii, i.e. 6 mm, 7 mm, 9 mm and 10 mm. It has been reported that to achieve an accurate solution the diameter of the smallest particle should cover at least 10 fluid grids. The fluid domain in this study is divided into 2000×2000 lattices with grid spacing $h = 0.5\,mm$. The ratio of smallest radius to grid spacing is 24 which can secure the accuracy of simulation. The time step used in this simulation is $8.333\times10^{-5}$ s. Other parameters of the fluid and solid particles are listed in Table 1. A pressure pipe (with pressure 125MPa) is applied in the middle of the left vertical wall. At the right boundary, a solid wall which is only effective for solid particles and a pressure boundary (with a density $\rho_{out} = 1000kg/m^3$) for the fluid are implemented. Other boundaries are stationary walls.

In 2-D simulation by combining DEM and other fluid method, like CFD and LBM, there is big issue in pore water flow path. Because the flow paths are always blocked up by contacted spheres, it is difficult to obtain realistic flow channels. In order to solve this problem, Boutt et al. (2007) proposed a method in which the radius of the particle will be reduced to certain degree (called effective radius) artificially when the fluid flow is implemented. This effective hydraulic radius can be accomplished by introducing a ratio of effective radius to the particle radius.

Fig. 6 shows the snapshots at different instants. The velocity contour of the fluid is displayed in colours. Due to the hydraulic loading in the middle of the left boundary, the onset and propagation of fracture, which is achieved by breaking the bond model between the particles undergoing too large forces, are captured. In order to better understand the mechanism of the onset and evolution of hydraulic fracturing, the bond network, similar to force chain in DEM, is extracted and its evolution is shown as well. The network is comprised of black and red lines. The former represents tension force between bonded particles and the latter is compression force or zero stress state. The magnitude of forces is described by the thickness of lines. At the beginning black tensile stresses appear near the hydraulic loading. With the growth of hydraulic loading tensile stresses propagate outward. When the tension is large enough, the bond breaks. Consequently, micro factures are formed.

To further observe the evolution of fracture induced by hydraulic loading, the zoom-in of fracture at different stages is delineated using green curves in Fig.7. At the beginning a tiny crack is formed near the pressure pipe. With the increase of fluid pressure, the hydraulic fracture grows gradually. Later, a branch fracture captured at t=0.8333s is formed and its width grows at t=1.6666s. Subsequently, a new branch emerges and these fractures propagate rapidly.

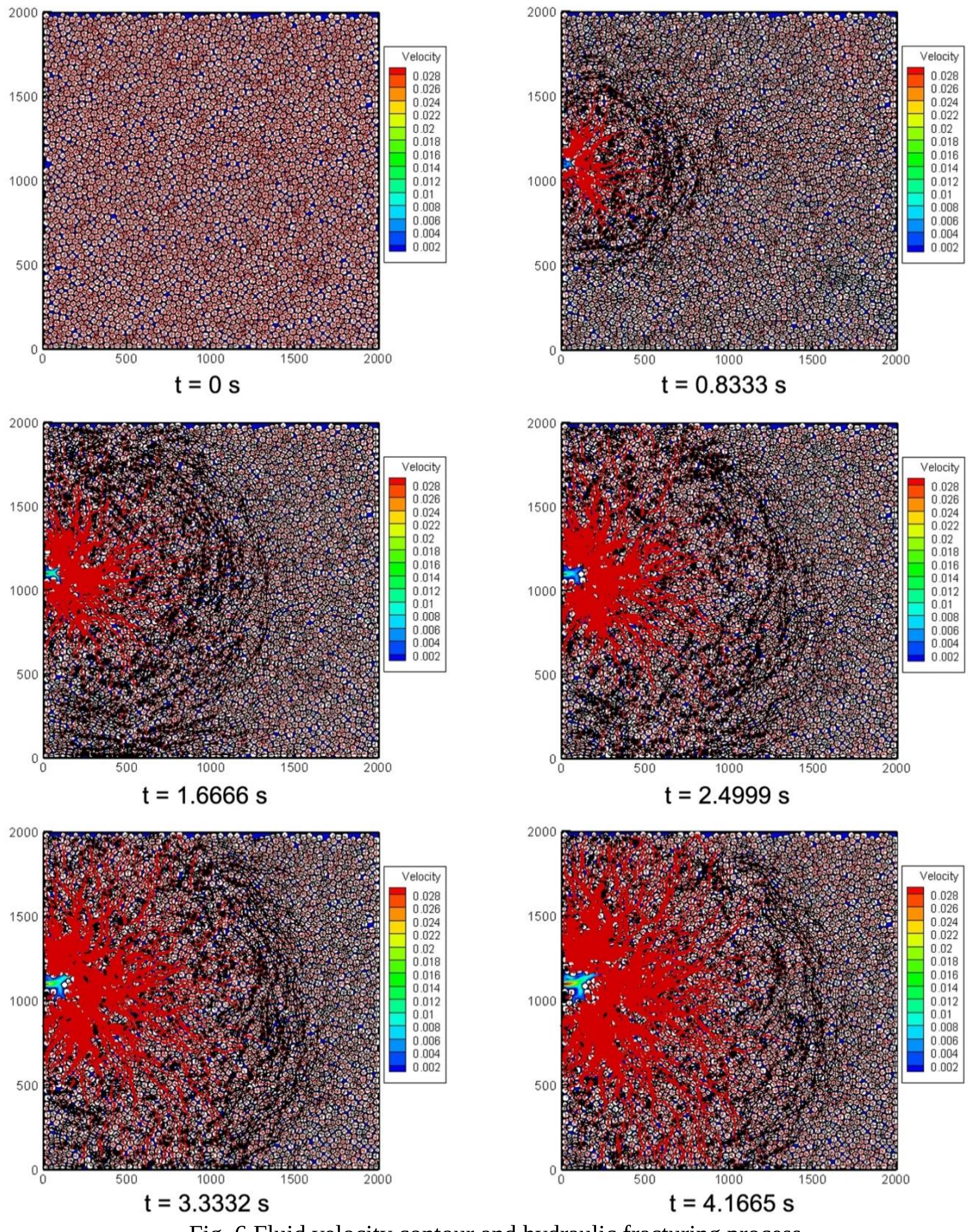


Fig. 6 Fluid velocity contour and hydraulic fracturing process

To trace the variation of fluid pressure, four points, (0.05, 0.55) (0.25, 0.55) (0.50, 0.55) and (0.75, 0.55), are selected and tracked. The distribution and evolution of fluid pressures are presented in Fig. 8, which shows that with the progress of the simulation, the pressures at all the points increase quickly. Particularly, the closer to the pressure pipe, the larger are the magnitude and speed of the growth of fluid pressure. Besides, the fluid pressure near the pressure pipe is higher than that far from hydraulic loading. With the increase of distance from the hydraulic loading, the fluid pressure drops dramatically.

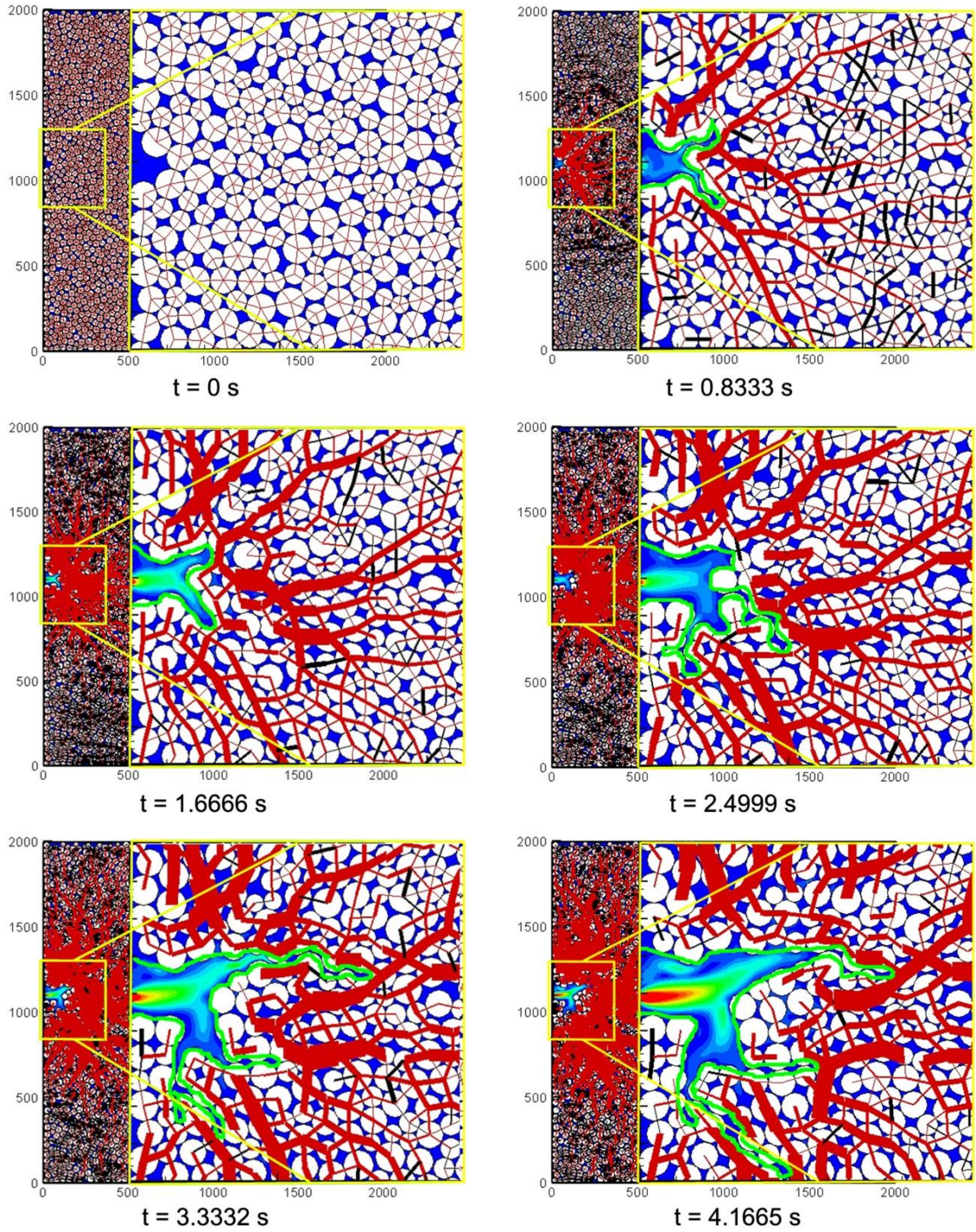


Fig. 7 Zoom-in of hydraulic fracture at different instants

The preliminary result demonstrates that this coupled BPLBM is promising for hydraulic fracture study where the experiments and conventional numerical methods have limited resolutions. It can investigate the hydraulic fracturing at the grain level and easily resolve the complicated interaction between the fracture surface and fluid. Besides, this microscopic method is particularly effective to and suitable for the investigation of fracture initiation and propagation through breaking the bonding between bonded particles. This advantage has been proven through the preliminary simulation. Particularly, the computing cost is very expensive. The hydraulic fracture simulation takes about 20 hours on a PC (Intel Core i7-4790 CPU@3.60GHz; Memory: 16.00 GB).

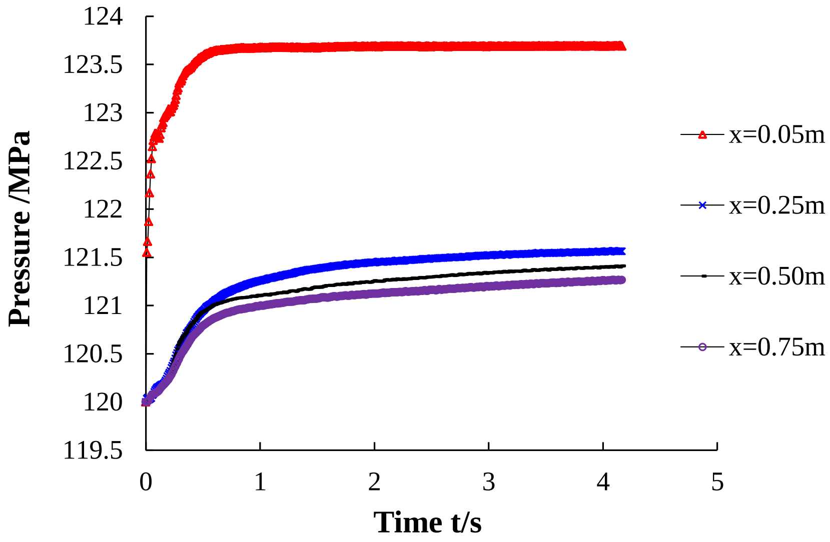


Fig. 8 Evolution of fluid pressure at different positions

## 5 Conclusions

This paper presents a novel coupled Bonded Particle and Lattice Boltzmann Method for the simulation of fluid-solid interactions in hydraulic fracturing. Numerical tests confirm that the coupled BPLBM technique is promising and efficient in capturing the onset and propagation of hydraulic fracture. Compared to DEM-LBM, it enjoys an improved accuracy and a broader range of applicability in characterizing the mechanics responses of geomaterials in which cohesion forces play an important role. Furthermore, BPLBM is a mesoscopic/microscopic based method, which can process fluid-particle issues at the grain-level which commonly ranges from hundreds of microns to several centimetres. This characteristic is difficult to achieve in a continuum based method. Due to the explicit time-stepping scheme and nature to parallelize, BPLBM is promising for modelling large-scale even field problems using parallel computing.

The present work only presents a 2D BPLBM technique, but the extension to 3D would be straightforward. Although only a simple bond model has been incorporated in BPLBM, advanced bond models able to resist moment will be developed and validated experimentally in the near future.

**References**


Ames, B. C. & Bunger, A. 2015. Role of Turbulent Flow in Generating Short Hydraulic Fractures With High Net Pressure in Slickwater Treatments. *SPE Hydraulic Fracturing Technology Conference*. The Woodlands, Texas, USA: Society of Petroleum Engineers.

Carter, B., Desroches, J., Ingraffea, A. & Wawrzynek, P. 2000. Simulating fully 3D hydraulic fracturing. *Modeling in geomechanics,* 200**,** 525-557.

Chen, H., Chen, S. & Matthaeus, W. H. 1992. Recovery of the Navier-Stokes equations using a lattice-gas Boltzmann method. *Phys, Rev. A,* 45**,** 5339-5342.

Chen, S., Chen, H., Martinez, D. O. & W. H. Matthaeus 1991. Lattice Boltzmann model for simulation of magnetohydrodynamics. *Phys. Rev. Lett.,* 67**,** 3776-3779.

Chen, Z. 2013. An ABAQUS Implementation of the XFEM for Hydraulic Fracture Problems. *ISRM International Conference for Effective and Sustainable Hydraulic Fracturing.* Brisbane, Australia: International Society for Rock Mechanics.

Cundall, P. A. & Strack, O. D. L. 1978. The distinct element method as a tool for research in granular media. *Report to the National Science Foundation Concerning NSF Grant ENG76-20711*.

Cundall, P. A. & Strack, O. D. L. 1979. A discrete numerical model for granular assemblies. *Geotechnique,* 29**,** 47-65.

Dash, S. M., Lee, T. S., Lim, T. T. & Huang, H. 2014. A flexible forcing three dimension IB–LBM scheme for flow past stationary and moving spheres. *Computers & Fluids,* 95**,** 159-170.

D'humieres, D., Ginzburg, I., Krafczyk, M., Lallemand, P. & Luo, L. S. 2002. Multiple-relaxation-time lattice Boltzmann models in three dimensions. *Philosophical Transactions of the Royal Society A: Mathematical, Physical and Engineering Sciences,* 360**,** 437-451.

Delenne, J.-Y., El Youssoufi, M. S., Cherblanc, F. & Bénet, J.-C. 2004. Mechanical behaviour and failure of cohesive granular materials. *International Journal for Numerical and Analytical Methods in Geomechanics,* 28**,** 1577-1594.

Feng, Y. T., Han, K. & Owen, D. R. J. 2007. Coupled lattice Boltzmann method and discrete element modelling of particle transport in turbulent fluid flows: Computational issues. *International Journal for Numerical Methods in Engineering,* 72**,** 1111-1134.

Feng, Y. T. & Owen, D. R. J. 2002. An augmented spatial digital tree algorithm for contact detection in computational mechanics. *International Journal for Numerical Methods in Engineering,* 55**,** 159-176.

Fu, P., Johnson, S. M. & Carrigan, C. R. 2013. An explicitly coupled hydro-geomechanical model for simulating hydraulic fracturing in arbitrary discrete fracture networks. *International Journal for Numerical and Analytical Methods in Geomechanics,* 37**,** 2278-2300.

Han, K., Feng, Y. T. & Owen, D. R. J. 2007. Coupled lattice Boltzmann and discrete element modelling of fluid-particle interaction problems. *Computers and Structures,* 85**,** 1080-1088.

Higuera, F. J. & Jiménez, J. 1989. Boltzmann Approach to Lattice Gas Simulations. *EPL (Europhysics Letters),* 9**,** 663-668.

Higuera, F. J., Succi, S. & Benzi, R. 1989. Lattice Gas Dynamics with Enhanced Collisions. *EPL (Europhysics Letters),* 9**,** 345-349.

Holdych, D. J. 2003. *Lattice Boltzmann methods for diffuse and mobile interfaces.* University of Illinois at Urbana.

Hossain, M. M. & Rahman, M. K. 2008. Numerical simulation of complex fracture growth during tight reservoir stimulation by hydraulic fracturing. *Journal of Petroleum Science and Engineering,* 60**,** 86-104.

Huidan, Y., Girimaji, S. S. & Li-Shi, L. 2005. DNS and LES of decaying isotropic turbulence with and without frame rotation using lattice Boltzmann method. *Journal of Computational Physics,* 209**,** 599-616.

Itasca Consulting Group Inc 2002. Particle Flow Code in 2 Dimensions. *version 3.0. Minnesota, U.S.A.*

Jiang, M. J., Sun, Y. G., Li, L. Q. & Zhu, H. H. 2012. Contact behavior of idealized granules bonded in two different interparticle distances: An experimental investigation. *Mechanics of Materials*, 55.

Jiang, M. J., Zhu, F., Liu, F. & Utili, S. 2014. A bond contact model for methane hydrate-bearing sediments with interparticle cementation. *International Journal for Numerical and Analytical Methods in Geomechanic*s, 38, 1823-1854.

Jones, B. 2013. Characterisation of porous media using the Lattice Boltzmann method. *Ph.D. thesis, Swansea University*.

Ladd, A. J. C. 1994. Numerical simulations of particulate suspensions via a discretized Boltzmann equation. Part 1. Theoretical foundation. *Journal of Fluid Mechanics,* 271**,** 285-309.

Ladd, A. J. C. & Verberg, R. 2001. Lattice-Boltzmann Simulations of Particle-Fluid Suspensions. *Journal of Statistical Physics,* 104**,** 1191-1251.

Luchi, M. L. & Rizzuti, S. 1987. Boundary elements for three-dimensional elastic crack analysis. *International Journal for Numerical Methods in Engineering,* 24**,** 2253-2271.

Ma, G. W., An, X. M., Zhang, H. H. & Li, L. X. 2009. Modeling complex crack problems using the numerical manifold method. *International Journal of Fracture,* 156**,** 21-35.

Mcnamara, G. R. & Zanetti, G. 1988. Use of the Boltzmann Equation to Simulate Lattice-Gas Automata. *Physical Review Letters,* 61**,** 2332-2335.

Moës, N., Dolbow, J. & Belytschko, T. 1999. A finite element method for crack growth without remeshing. *International Journal for Numerical Methods in Engineering,* 46**,** 131-150.

Mohammadnejad, T. & Khoei, A. R. 2013. An extended finite element method for hydraulic fracture propagation in deformable porous media with the cohesive crack model. *Finite Elements in Analysis and Design,* 73**,** 77-95.

Munjiza, A. 2004. The Combined Finite-Discrete Element Method. London.

Munjiza, A. & Andrews, K. R. F. 1998. NBS contact detection algorithm for bodies of similar size. *International Journal for Numerical Methods in Engineering,* 43**,** 131-149.

Munjiza, A., Owen, D. R. J. & Bicanic, N. 1995. A combined finite-discrete element method in transient dynamics of fracturing solids. *Engineering Computations,* 12**,** 145-174.

Noble, D. R. & Torczynski, J. R. A lattice-Boltzmann method for partially saturated computational cells. 1998 Singapore. World Scientific, 1189-1201.

Owen, D. R. J. & Feng, Y. T. 2001. Parallelised finite/discrete element simulation of multi-fracturing solids and discrete systemsnull. *Engineering Computations,* 18**,** 557-576.

Potyondy, D. O. 2007. Simulating stress corrosion with a bonded-particle model for rock. *International Journal of Rock Mechanics and Mining Sciences,* 44**,** 677-691.

Potyondy, D. O. & Cundall, P. A. 2004. A bonded-particle model for rock. *International Journal of Rock Mechanics and Mining Sciences,* 41**,** 1329-1364.

Qian, J., Zhan, H., Luo, S. & Zhao, W. 2007. Experimental evidence of scale-dependent hydraulic conductivity for fully developed turbulent flow in a single fracture. *Journal of Hydrology*, 339, 206-215.

Smagorinsky, J. 1963. General circulation experiments with the primitive equations. *Monthly Weather Review,* 91**,** 99-164.

Strack, O. E. & Cook, B. K. 2007. Three-dimensional immersed boundary conditions for moving solids in the lattice-Boltzmann method. *International Journal for Numerical Methods in Fluids,* 55**,** 103-125.

Tsai, V. C. & Rice, J. R. 2010. A model for turbulent hydraulic fracture and application to crack propagation at glacier beds. *Journal of Geophysical Research: Earth Surface*, 115, F03007.

Tsai, V. C. & Rice, J. R. 2012. Modeling Turbulent Hydraulic Fracture Near a Free Surface. *Journal of applied mechanics*, 79, 031003.

Zhang, G., Li, X. & Li, H. 2015. Simulation of hydraulic fracture utilizing numerical manifold method. *Science China Technological Sciences***,** 1-16.

**Table 1 Parameters for the fluid and solid**

| Parameter | Value | Parameter | Value |
|---|---|---|---|
| Particle density (kg/m$^3$) | 2750 | Fluid density (kg/m$^3$) | 1000 |
| Friction coefficient | 0.3 | kinematic viscosity ($\upsilon$) | $1.0\times10^{-6}$ |
| Particle contact stiffness (N/m) | $5.0\times10^{7}$ | Bond normal stiffness (N/m) | $5.0\times10^{7}$ |
| Bond strength (N) | 1500 | Bond shear stiffness | $1.0\times10^{5}$ |
| Contact damping ratio ($\xi$) | 0.5 | Smagorinsky constant ($S_c$) | 0.1 |

**Figures list**